





Article

Correlation between Ground Measurements and UAV Sensed Vegetation Indices for Yield Prediction of Common Bean Grown under Different Irrigation Treatments and Sowing Periods

Aleksa Lipovac ^{1,*}, Atila Bezdán ², Djordje Moravčević ¹, Nevenka Djurović ¹, Marija Ćosić ¹, Pavel Benka ² and Ružica Stričević ¹

¹ Faculty of Agriculture, University of Belgrade, Nemanjina 6, 11080 Belgrade, Serbia

² Faculty of Agriculture, University of Novi Sad, Dositeja Obradovića 8, 21000 Novi Sad, Serbia

* Correspondence: alipovac@agrif.bg.ac.rs

Abstract: The objective of this study is to assess the possibility of using unmanned aerial vehicle (UAV) multispectral imagery for rapid monitoring, water stress detection and yield prediction under different sowing periods and irrigation treatments of common bean (*Phaseolus vulgaris*, L). The study used a two-factorial split-plot design, divided into subplots. There were three sowing periods (plots; I—mid April, II—end of May/beginning of June, III—third decade of June/beginning of July) and three levels of irrigation (subplots; full irrigation (F)—providing 100% of crop evapotranspiration (ET_c), deficit irrigation (R)—providing 80% of ET_c , and deficit irrigation (S) providing—60% of ET_c). Canopy cover (CC), leaf area index (LAI), transpiration (T) and soil moisture (Sm) were monitored in all treatments during the growth period. A multispectral camera was mounted on a drone on seven occasions during two years of research which provided raw multispectral images. The NDVI (Normalized Difference Vegetation Index), MCARI1 (Modified Chlorophyll Absorption in Reflectance Index), NDRE (Normalized Difference Red Edge), GNDVI (Green Normalized Difference Vegetation Index) and Optimized Soil Adjusted Vegetation Index (OSAVI) were computed from the images. The results indicated that NDVI, MCARI1 and GNDVI derived from the UAV are sensitive to water stress in S treatments, while mild water stress among the R treatments could not be detected. The NDVI and MCARI1 of the II-S treatment predicted yields better ($r^2 = 0.65$, $y = 4.01 \text{ tha}^{-1}$; $r^2 = 0.70$, $y = 4.28 \text{ tha}^{-1}$) than of III-S ($r^2 = 0.012$, $y = 3.54 \text{ tha}^{-1}$; $r^2 = 0.020$, $y = 3.7 \text{ tha}^{-1}$). The use of NDVI and MCARI will be able to predict common bean yields under deficit irrigation conditions. However, remote sensing methods did not reveal pest invasion, so good yield predictions require observations in the field. Generally, a low-flying UAV proved to be useful for monitoring crop status and predicting yield and water stress in different irrigation regimes and sowing period.

Keywords: common bean; irrigation; late sowing; remote sensing; vegetation indices; yield prediction



Citation: Lipovac, A.; Bezdán, A.; Moravčević, D.; Djurović, N.; Ćosić, M.; Benka, P.; Stričević, R. Correlation between Ground Measurements and UAV Sensed Vegetation Indices for Yield Prediction of Common Bean Grown under Different Irrigation Treatments and Sowing Periods. *Water* **2022**, *14*, 3786. <https://doi.org/10.3390/w14223786>

Academic Editor: Guido D'Urso

Received: 7 October 2022

Accepted: 18 November 2022

Published: 21 November 2022

Publisher's Note: MDPI stays neutral with regard to jurisdictional claims in published maps and institutional affiliations.



Copyright: © 2022 by the authors. Licensee MDPI, Basel, Switzerland. This article is an open access article distributed under the terms and conditions of the Creative Commons Attribution (CC BY) license (<https://creativecommons.org/licenses/by/4.0/>).

1. Introduction

One of the major challenges in the 21st century will be to enhance agriculture despite climate change, in order to meet the increasing food demand due to population growth. Air temperature increase, redistribution and varying intensity of rainfall, drought, and water scarcity are the most severe threats to crop farming [1–3], indicating that the agricultural sector will be the most threatened by climate change.

In that regard, various improvements and innovations in agriculture sector (irrigation strategies and techniques [4–11]; fertilization [12–14] or field management practices [15–18], etc.) have already enhanced farming technologies, increased yields, and expanded the scope of farming while preserving soil and water. However, the principles of precision agriculture are being followed more widely to improve crop productivity and the use of natural resources.

Timely decisions and agrotechnical measures are increasingly based on information that characterizes the plot of land and the crop, derived from in situ observations and laboratory analyses. The monitoring of crop status with regard to water availability, nutrient supply, and health is conducted using ground-based devices, such as leaf area index sensors [19], thermal cameras [20,21] leaf water potential chambers [22–24] and the like. These methods are accurate but time consuming in the field and unsuitable for large areas because they cannot provide an overall picture.

As such, a lot of research is focused on the potential of remote sensing for monitoring the status of crops over space and time. The various specific applications of remote sensing are (e.g., yield prediction, water status and irrigation, weed detection, fertilization, precision farming etc.) on the primary platforms (e.g., unmanned aerial vehicles—UAV, satellite, and sensors) [25–27]. Irrigation management using satellites was developed and widely researched [28–30]. Remote sensing by means of a small unmanned aerial vehicle (UAV) with high spatial resolution is increasingly used to precisely assess the crop water status [31], yield [32], biomass [33], leaf area index (LAI) [34], and stress [35]. To date, the deployment of UAVs for irrigation practices has been studied extensively but can still be improved [36]. Mwinuka et al. [31] used multispectral and thermal images to determine irrigated plant water conditions and predict yields of the African eggplant. They emphasized the Normalized Difference Vegetation Index (NDVI) and Optimized Soil Adjusted Vegetation Index (OSAVI) for water stress detection and yield prediction. Kirnak and Hasan [24] reported strong correlations between LAI, leaf water potential (LWP), and seed yield (SY) with nine different spectral vegetation indices on drip irrigated pumpkin, indicating that VI could be useful for yield estimation and irrigation scheduling. Nemeskeri et al. [37] proved that NDVI measured during flowering and pod development correlates closely with yields of snap bean. Vegetation indices (NDVI, Green Normalized Difference Vegetation Index (GNDVI), and Blue Normalized Difference Vegetation Index (BNDVI)) acquired from UAV could detect the water stress of turf grass before it occurs, suggesting that weekly measurements with UAV could benefit irrigation management [38]. Irrigation management using NDVI proved to be effective under variable-rate irrigation systems [39].

There are only a few studies related to the usage of the UAVs for irrigation management and yields estimation of bean cultivars (*Phaseolus vulgaris*). Zhou et al. [40] proposed GNDVI and canopy cover from multispectral sensed data as crop water stress and seed yield indicators of pinto beans. Koksai et al. [41] conducted a study on common bean grown in a subhumid climate in an optimal sowing period and determined that spectral reflectance values were influenced by different irrigation regimes and vegetation conditions. They indicated that these variations offered significant possibilities for the use of remote sensing in the estimation of ET_a (actual evapotranspiration). Common bean biomass and GNDVI strongly correlated and could be used for the monitoring of common bean drought stress [42].

Additionally, Rai et al. [43] and Ranjan et al. [44] evaluated the role of ground-based vegetation indices (VIs) for irrigated pinto bean stress and yield assessments.

Remote sensing based on UAVs, along with farming technologies with different irrigation treatments and sowing periods, suggests significant potential for improving agriculture on a farmer scale from the viewpoints of optimal yield, maximized soil utilization, and water conservation. Vegetation indices can help farmers make accurate decisions about proper crop management, as well as in detecting crop stress response and predicting yield. The production of beans in Serbia is declining and is characterized by low and variable yields (roughly 1 t ha^{-1}) [45], which leads to increasing imports and high prices of beans in the market.

Therefore, our research objective was to evaluate the ability of the early detection of water stress of the common bean (*Phaseolus vulgaris* L.) with three different irrigation regimes from well-watered to severe deficit irrigation using UAV in three different sowing periods (from mid-April to the beginning of July). Another objective was to analyze

the correlation between canopy cover (CC), leaf area index (LAI), transpiration (T), soil moisture (Sm) and vegetation indices (VI) obtained with UAV in different irrigation regimes and different sowing periods. Specifically, our goal was to determine whether UAV could be used for rapid yield prediction under different water supply conditions of the common bean (*Phaseolus vulgaris*, L) grown in different periods of the year.

2. Materials and Methods

2.1. Study Area

The experiment was conducted in 2019 and 2020 in an open field of the farm Napredak AD, belonging to the company Delta Agrar. The study area is located near the town of Stara Pazova, some 40 km north of Belgrade, Serbia (latitude 44°58'50.29"; longitude 20°7'45.16"; 79 m above sea level), in southeast Europe (Figure 1). The climate in the area is moderate continental. The average annual air temperature is 12.4 °C, the warmest months are July and August (avg. 22.9 °C), and the coldest months are December and January (avg. 1.1 °C). The average humidity is 74.3%, and the range is from 86.3% (high) to 65.6% and 65.2% (low), corresponding the lowest and highest average air temperatures, respectively. The average wind speed at 2 m is 1.8 ms⁻¹ and the windiest month is March (2.2 ms⁻¹). The annual average precipitation is 620 mm, varying from 937.3 mm to 351.6 mm. The wettest month is June (79.7 mm) and the driest is February (33.2 mm). According to the official soil classification system of Serbia, the soil in the study area is Chernozem with an A-AC-CA-C profile [46]. Based on the US classification [47], the soil in horizon A (0–55 cm) is silt loam, in horizons AC (55–90 cm) and CA (90–115 cm) it is silt clay loam, and in horizon C it is silty loam. The soil air-water characteristics are favorable along the entire depth. The field capacity is uniform, ranging from 33.94% to 32.07%. The bulk density of the soil in horizon A is 1.22 gcm⁻³ and increases with depth to 1.4 gcm⁻³ (C). The humus content decreases with depth and is the highest in the humus-accumulative horizon A (3.62%).



Figure 1. Location of study area.

The content of total nitrogen in the surface horizon is 0.18%. The concentration of plant available potassium (K) in A horizon is 0.03%, and the concentration of plant available phosphorus (P) is 0.16%, which is indicative of high concentrations of these elements in the layer of soil that hosts the main part of the root system. Agrotechnical measures relating to weed, disease and pest control were standard, as generally applied in the research area.

2.2. Experiment Design

The two-year experiment was of a two-factorial split-plot design, divided into subplots. There were three sowing periods (plots) and three levels of irrigation (subplots) (Figure 2).

		Sowing date		
		I	II	III
Irrigation treatments	F	IF1	IIF1	IIIF1
		IF2	IIF2	IIIF2
		IF3	IIF3	IIIF3
	R	IR1	IIR1	IIIR1
		IR2	IIR2	IIIR2
		IR3	IIR3	IIIR3
	S	IS1	IIS1	IIIS1
		IS2	IIS2	IIIS2
		IS3	IIS3	IIIS3

Figure 2. Design of the experiment.

Irrigation treatments included full irrigation, providing 100% of ET_c (evapotranspiration of the crop) (F); deficit irrigation at approximately 80% of ET_c (R), and deficit irrigation at approximately 60% of ET_c (S). The same irrigation depth was applied in all irrigation treatments, but the irrigation interval varied between the treatments. Full irrigation (F) was applied in three-day intervals and deficit irrigation R and S in four- and five-day intervals, respectively. Irrigation depth varied from 12 to 18 mm due to the available soil water content, sowing period, the phenological stage of the crop, and evapotranspiration.

The irrigation water was withdrawn from an artesian well located in the immediate vicinity of the experimental field. The method was drip irrigation. Drip tapes manufactured by Rivulis were used. The spacing between the emitters was 0.2 m, the spacing between the drip tapes was 0.5 m (each row was irrigated by one drip tape), and the flow rate of each emitter was 1.1 lh^{-1} . Irrigation timing was adjusted to achieve the desired irrigation depth. Upon sowing, the parcels were irrigated to field capacity to ensure favorable conditions for germination and sprouting of the common bean. Table 1 shows the irrigation depth per sowing period. There were three sowing periods: standard I (mid-April, consistent with climate conditions in Serbia), late II (end of May/beginning of June), and late III (third decade of June/beginning of July).

Table 1. Irrigation treatments of common bean.

Year	Irrigation Treatment/Sowing Period	I		II		III	
		Irrigation Depth (mm)	Irrigation Events	Irrigation Depth (mm)	Irrigation Events	Irrigation Depth (mm)	Irrigation Events
2019	F	0	0	150	9	249	15
	R	0	0	117	7	180	11
	S	0	0	84	5	129	8
2020	F	228	14	141	9	200	13
	R	162	10	90	6	144	9
	S	126	8	75	5	111	7

Figure 3 shows the duration of growth by sowing period. The sowing dates varied depending on weather conditions. The amount and distribution of rainfall sometimes delayed the sowing of the late crops.

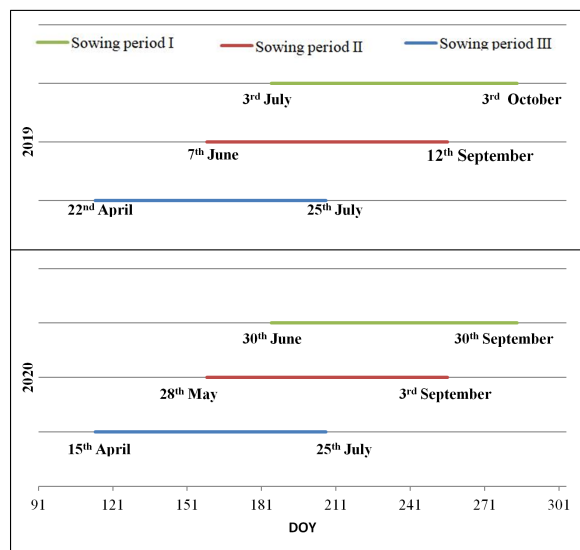


Figure 3. Growing season of common bean and sowing dates of the experiment.

2.3. Ground Monitoring

2.3.1. Meteorological Observations

An automatic weather station of the company EMS Brno was installed in the experimental field to monitor climate parameters and calculate reference evapotranspiration (ET_0). The station was located on a representative spot, in the immediate vicinity of the plots, on grass that was irrigated, cut and maintained during the season.

2.3.2. Evapotranspiration

Crop evapotranspiration (ET_c) was calculated for all sowing periods and irrigation treatments.

For an accurate estimation of a specific crop water use in real time, evaporation and transpiration need to be considered separately. ET_c was determined by multiplying reference evapotranspiration (ET_0) and the dual crop coefficient (K_c). Reference evapotranspiration was calculated using the FAO Penman-Monteith method. Daily values of weather parameters were obtained from the previously mentioned weather station.

$$ET_c = ET_0 \times (K_{cb} + K_e) \quad (1)$$

where ET_c is the crop evapotranspiration (mm), ET_0 is the reference evapotranspiration (mm), K_{cb} the basal crop coefficient (obtained from FAO Irrigation and drainage paper 56) [48], and K_e is the soil evaporation coefficient.

The soil evaporation coefficient (K_e) was calculated by estimating the available energy and soil moisture regimes at the soil surface in the original FAO-56 procedure [48]:

$$K_e = K_r \cdot (K_{cmax} - K_{cb}) \leq f_{ew} \cdot K_{cmax} \quad (2)$$

where K_{cmax} is the maximum value of K_c following rain or irrigation; K_r is the evaporation reduction coefficient dependent on the cumulative depth of water depleted (evaporated); and f_{ew} is the fraction of the soil that is both exposed to solar radiation and that is wetted (0.01–1.0).

K_{cmax} represents the upper limit of evaporation from any cropped surface and is adjusted for crop height and climate:

$$K_{c\ max} = \max \left(\left\{ \left[1.2 + [0.04 \times (u_2 - 2) - 0.004 \times (RH_{min} - 45)] \times \left(\frac{h_c}{3} \right)^{0.3} \right] \right\}, \{K_{cb} + 0.05\} \right) \quad (3)$$

where u_2 represents the wind speed (ms^{-1}) measured at a height of 2 m; RH_{min} is the minimum daily relative humidity (%); and h_c is the crop height (m)

The evaporation reduction coefficient (k_r) is dependent on soil water depletion from the topsoil layer:

$$K_r = \frac{TEW - D_{e,i-1}}{TEW - REW} \quad (4)$$

where $D_{e,i-1}$ is the cumulative depth of evaporation from the soil surface layer at the end of day $i - 1$ (the previous day) (mm); TEW , total evaporable water, is the maximum cumulative depth of evaporation from the soil surface layer when $K_r = 0$ (mm); REW , readily evaporable water, is the value obtained from the FAO Irrigation and drainage paper (56) for silt loam soils, namely 10 mm up to a depth of 10 cm. When $D_{e,i-1} \leq REW$, $K_r = 1.0$.

$$TEW = 1000 \times (W_{FC} - 0.5\theta_{WP}) \times Z_e \quad (5)$$

where W_{FC} is the soil water content at field capacity ($\text{m}^3 \text{m}^{-3}$); θ_{WP} is the soil water content at wilting point in the topsoil layer ($\text{m}^3 \text{m}^{-3}$); and Z_e is the depth of the topsoil layer that is subjected to evaporation (m), i.e., 0.1–0.15 m is recommended for row crops in Allen et al. (1998).

The calculation of k_r requires the daily water budget for the exposed and wetted surface to determine D_e :

$$D_{e,i-1} = ET_0 \times K_e - (P_i + I_i - DP_i) \quad (6)$$

where $D_{e,i-1}$ is the cumulative depth of evaporation of the topsoil at the end of day i and $i - 1$ (mm); P_i is the precipitation on day i (mm); I_i is the irrigation depth on day i that infiltrates the soil (mm); and DP_i is deep percolation on day i .

In R and S treatments, the plants were not well-supplied with water, therefore the stress coefficient (K_s) was calculated [48]:

$$ET_a = ET_0 \times (K_s \times K_{cb} + K_e) \quad (7)$$

where K_s is the water stress coefficient, and it depends on available soil water in the root zone.

$$K_s = \frac{TAW - D_{r,i-1}}{TAW - RAW}$$

where $D_{r,i-1}$ is root zone depletion at the end of day $i - 1$ (mm); TAW is the total available soil water in the root zone (mm); and RAW is the readily available soil water in the root zone (mm). When $D_{r,i-1} < RAW$, $K_s = 1.0$.

$$TAW = (\theta_{FC} - \theta_{WP}) \times Z_r \quad (8)$$

where Z_r is the rooting depth (m).

The calculation of $D_{r,i-1}$ requires the daily water budget for the root zone, as with Equation

$$D_{r,i} = D_{r,i-1} - P_i - I_i - DP_i + ET_{c,i} \quad (9)$$

where $D_{r,i}$ and $D_{r,i-1}$ are cumulative depths of transpiration in the root zone at the end of day i and $i - 1$ (mm), respectively; and $ET_{c,i}$ is crop evapotranspiration on day i (mm).

To accurately assess the effect of treatments on water use, additional calculations were made applying the water budgeting method, using available rainfall, irrigation depth, deep percolation and soil moisture variation data.

$$ETa = \frac{P + I + \Delta\theta - DP}{n} \quad (10)$$

where ETa is actual evapotranspiration (mmday^{-1}), I —irrigation (mm), $\Delta\theta$ —soil moisture variation between two measurements (mm), and n —number of days between two measurements.

2.3.3. Soil Moisture

The soil moisture (Sm) was measured by the standard gravimetric method on each subplot every 7–10 days. The soil was sampled by layer, at 0–20, 20–40 and 40–60 after heavy rainfall. The objective was the determining of the variations in soil water by sowing period and irrigation treatment, as well as identifying any correlation with vegetation indices.

2.3.4. Canopy Cover (CC)

The canopy cover was monitored by photographing elementary (1 m^2) subplots every 10–15 days, depending on weather conditions. Python in a JupyterLab environment (Figure 4), developed for this particular purpose (available on demand), was used to analyze the images. The results were presented as a percentage of the leaf area in the image that covers exactly 1 m^2 .

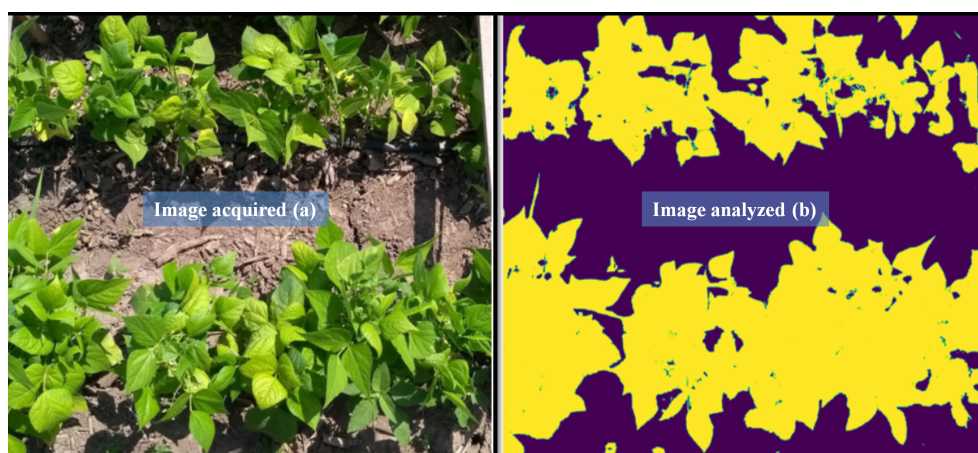


Figure 4. Canopy cover analysis.

2.3.5. Leaf Area Index (LAI)

The leaf area was measured by an LI-3100C area meter in the same subplots and time intervals as the canopy cover.

2.4. Vegetation Indices (VI) Determined from UAV Multispectral Imagery

2.4.1. UAV Image Acquisition

The images were captured by a Micasense RedEdge MX sensor (MicaSense, Inc., Wichita, KS, USA, <http://www.micasense.com/> accessed on 30 May 2022), installed in a DJI PHANTOM 4 PRO V2 drone. Each dataset contained five spectral bands: blue, green, red, red edge, and near infrared (Table 2). The selected flight altitude was 50 m and the spatial resolution was 3.7 cm. Before and after each flight, an image of the Calibrated Reflectance Panel was taken, enabling more accurate compensation for incident light conditions and the generation of quantitative data.

Table 2. Band and spatial resolution parameters of the multispectral data.

Band Number	Band Name	Spatial Resolution (cm)	Wavelength Range (Micrometer)	Central Wavelength (Micrometer)
1	Blue		0.465–0.485	0.475
2	Green		0.550–0.570	0.560
3	Red	3.7	0.663–0.673	0.668
4	Red edge		0.712–0.722	0.717
5	Near infrared		0.820–0.860	0.840

The UAV was deployed on sunny days, between 11:00 a.m. and 1:00 p.m. There were seven sorties during the study period (Table 3). Prior to image acquisition, the canopy cover was measured by treatment, the plants were sampled for LAI determination, and the soil was sampled for soil moisture measurement.

Table 3. Image acquisition dates during the study period.

Year 1	Year 2
4 July 2019	3 July 2020
19 July 2019	27 August 2020
16 August 2019	16 September 2020
13 September 2019	

2.4.2. Image Processing and Computation of Vegetation Indices

Pix4Dmapper (<https://www.sensefly.com/software/pix4d/> accessed on 30 May 2022) software was used to generate an orthomosaic from raw aerial images. Pix4Dmapper also served to correct the geometry in parallel. The final product was five different spectral bands in geoTIFF format.

QGIS 3.12 software was used for further processing. The images were trimmed to the level of experimental subplots with the Clipper application. The same software was employed to compute the indices by the Raster Calculator. Relevant statistical data per treatment were calculated using the Zonal Statistics tool and exported to xlsx. Calculated Vis are represented in the Table 4.

Table 4. Vegetation indices computed from multispectral bands.

Index	Equation	Reference
Normalized Difference Vegetation Index	$NDVI = \frac{NIR-RED}{NIR+RED}$	[49]
Modified Chlorophyll Absorption in Reflectance Index	$MCARI1 = 1.2(2.5(NIR - RED) - 1.3(NIR - GREEN))$	[50]
Normalized Difference Red Edge	$NDRE = \frac{NIR-REEDGE}{NIR+REEDGE}$	[51]
Green Normalized Difference Vegetation Index	$GNDVI = \frac{NIR-GREEN}{NIR+GREEN}$	[52]
Optimized Soil Adjusted Vegetation Index	$OSAVI = \frac{NIR-RED}{NIR+RED+0.16}$	[53]

2.5. Data Processing

Variance analysis (ANOVA) was used to determine the sensitivity of the vegetation indices to variations in the parameters monitored during the experiment (Y, LAI, CC, T and Sm), for different sowing periods and irrigation treatments. SAS software [54] was employed for this purpose. The LSD test (5% and 1% probabilities) was applied to test the differences between the treatments. Correlations between the VIs and the measured parameters were determined based on Pearson's correlation coefficients (r). The spatial variations in the normalized difference vegetation index (NDVI) by sowing period and irrigation treatment were analyzed.

Yields were predicted by modeling the equation of linear regression between the VIs and the yields achieved in the first year of research. Second-year yields were used to test model reliability, deriving a regression correlation between the predicted and achieved yields. The yield prediction performance of the regression equation was assessed by calculating yields and the coefficient of determination (r^2).

3. Results

3.1. Climate

Figure 5a,b show the daily high, low and mean air temperatures and precipitation levels. In 2019, the temperatures were 25.22 °C, 13.57 °C and 19.29 °C, respectively, for the first period (I); 30.17 °C, 15.80 °C, and 22.98 °C for the second period (II) and 28.12 °C, 13.54 °C, and 20.83 °C for the third period (III), respectively. The largest amount of rainfall was observed in period I (426.00 mm), followed by II (239.00 mm) and III (171.50 mm). No irrigation was applied in period I due to the large amount of rainfall. In 2020, the average high, low and mean daily air temperatures were 24.46 °C, 11.25 °C, and 18.11 °C in period I. Similar to the previous year, these temperatures were 28.45 °C, 15.25 °C, and 22.00 °C in period II, and 28.56 °C, 14.17 °C, and 21.62 °C in period III, respectively. The largest amount of rainfall was recorded in period II (280.00 mm), followed by I (246.80 mm) and III (210.00 mm). In general, the amounts of rainfall were high in both years and in all the sowing periods, but the highest was recorded in the first period of 2019 (426 mm).

3.2. Transpiration and Evaporation

Figure 6 shows transpiration levels (T) in both years by sowing period. In 2019 (Figure 6a), the lowest transpiration level was recorded in period I (314.93 mm) and was uniform irrespective of irrigation. Namely, the crop was rainfed because of rainy and cloudy weather. In period II, T was 346.24 mm, 312.42 mm and 243.48 mm for irrigation treatments F, R and S, respectively. In period III, the corresponding levels of T were 309.35 mm, 297.80 mm, and 274.80 mm. In 2020 (Figure 6b), the transpiration levels in period I were 398.81 mm, 373.81 mm and 353.27 mm for F, R and S, respectively. In period II, T was 433.60 mm, 389.2 mm and 377.50 mm for F, R and S, respectively. In period III, the corresponding levels of T were 337.30 mm, 292.60 mm, and 285.5.0 mm, respectively. The high T was as expected due to the higher stomatal conductance of the irrigated common bean [55].

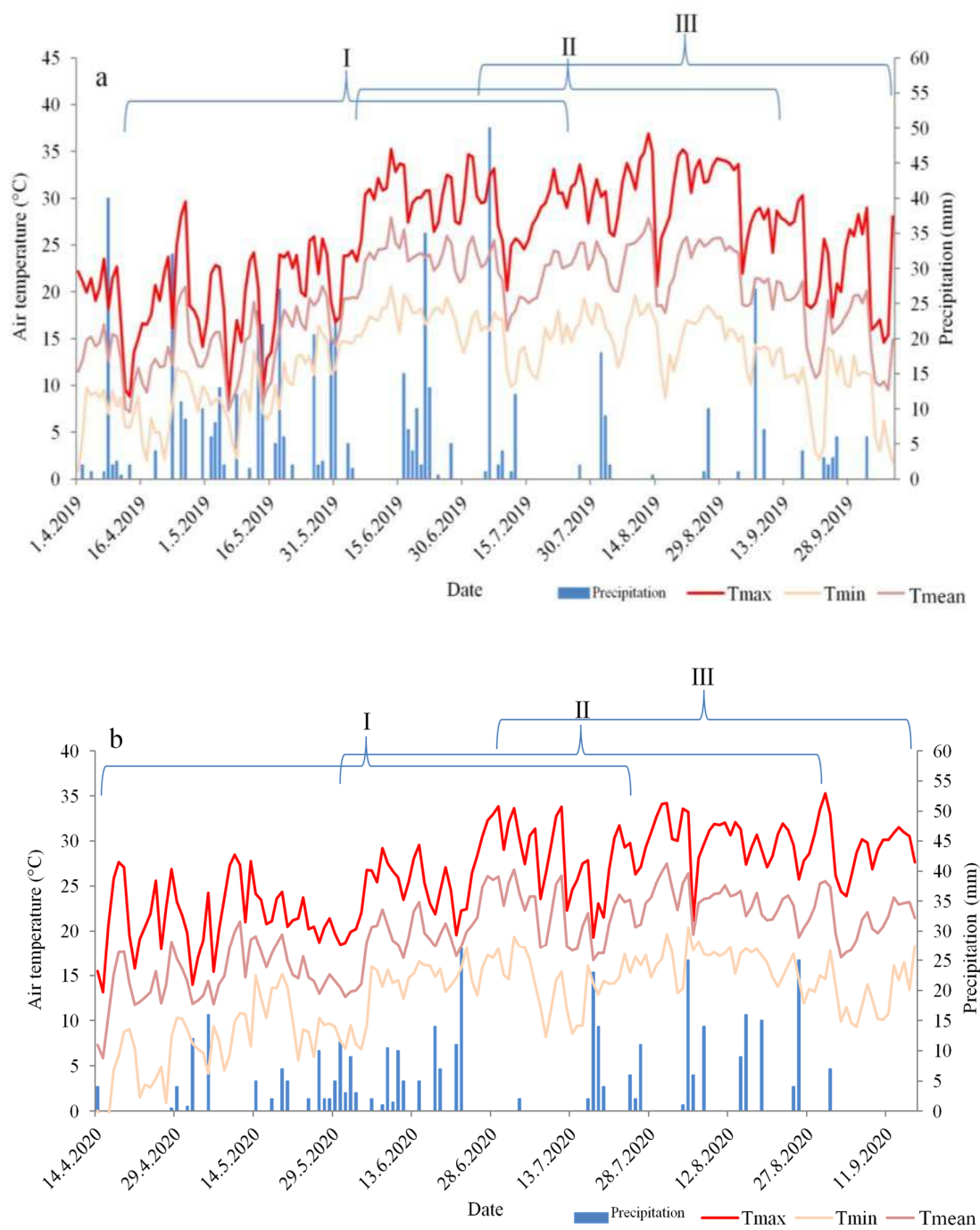


Figure 5. (a) Daily maximum, minimum and mean air temperatures and precipitation in 2019 for three sowing periods (I, II and III). (b) Daily maximum, minimum and mean temperatures and precipitation in 2020 for three sowing periods (I, II and III).

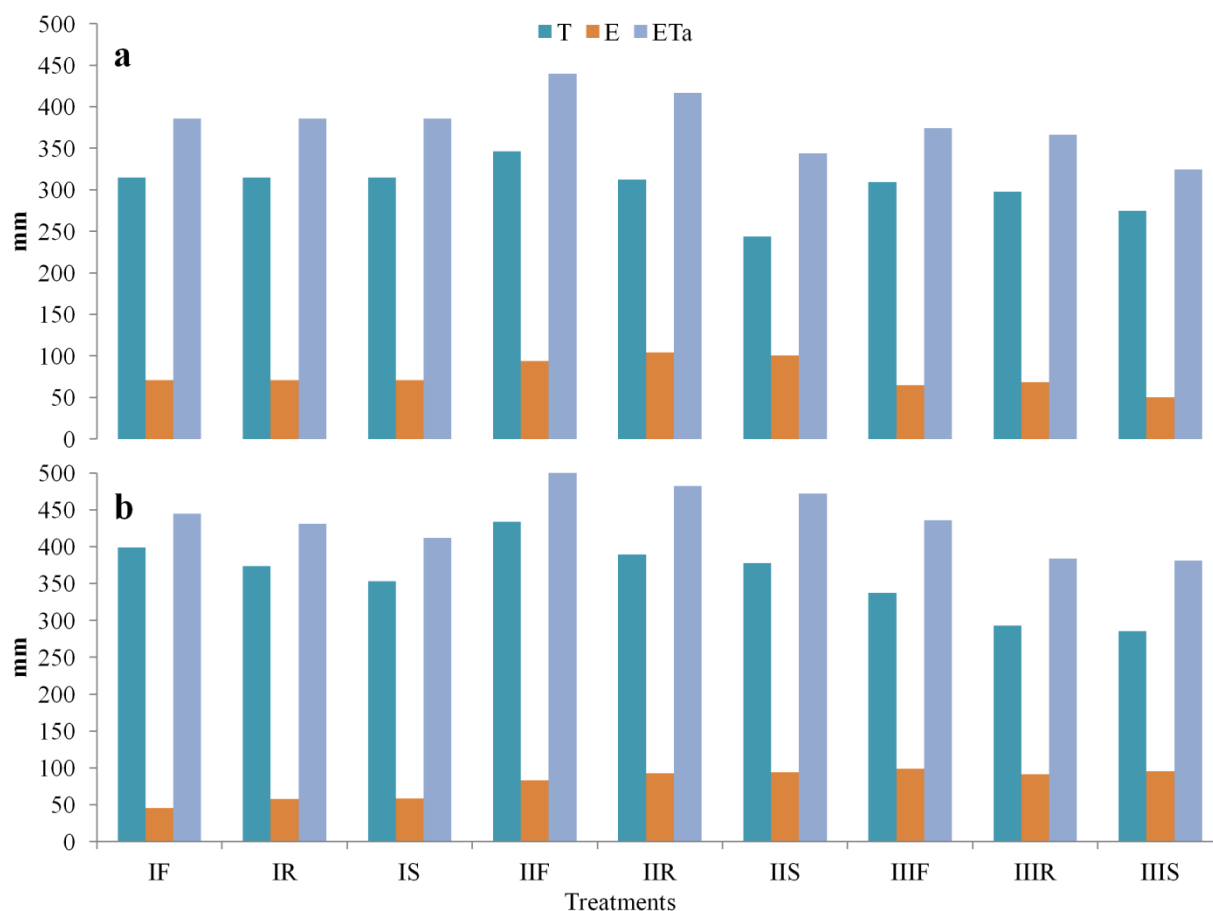


Figure 6. Evapotranspiration by irrigation treatment and sowing periods, calculated via the dual coefficient (IF, IR, IS, IIF, IIR, IIS, IIIF, IIIR, and IIIS): Three sowing periods (I, II and III), Actual evapotranspiration (ETa), evaporation (E), transpiration (T), full irrigation (F), deficit irrigation R, and deficit irrigation S in 2019 (a) and 2020 (b).

On average, evaporation was higher than transpiration 24 days after sowing in period I, 17 days in period II, and 15 days in period III. The highest evaporation averages were recorded in period II (94.8), which were significantly higher than in period III (78.2) and period I (62.6 mm). The plants comparable results for late sowing were reported by Srivastava et al. [56] for maize and Lipovac et al. [57] for common bean.

Figure 7 shows daily actual evapotranspiration (ETa), precipitation (P) and deep percolation (DP) for the three sowing periods and the F irrigation treatment. Figure 7 illustrates how rain events affected the evapotranspiration and the occurrence of deep percolation. Frequent and heavy rainfall events reduce actual evapotranspiration values due to the lowering of the temperature and high cloudiness, but also lead to deep percolation. Such phenomena were representative of both years of research. However, during the first year (2019), multi-day rainfall caused a significant fluctuation of actual evapotranspiration, and the values of deep percolation amounted to 147 mm, 62 mm and 54 mm in sowing periods I, II and III, respectively. High and multi-day rainfall in the first sowing period of 2019 caused the highest values of deep percolation. During 2020, due to better distributed rainfall of lower intensity, deep percolation ranged from 34 mm to 26 mm in sowing periods I and III, respectively.

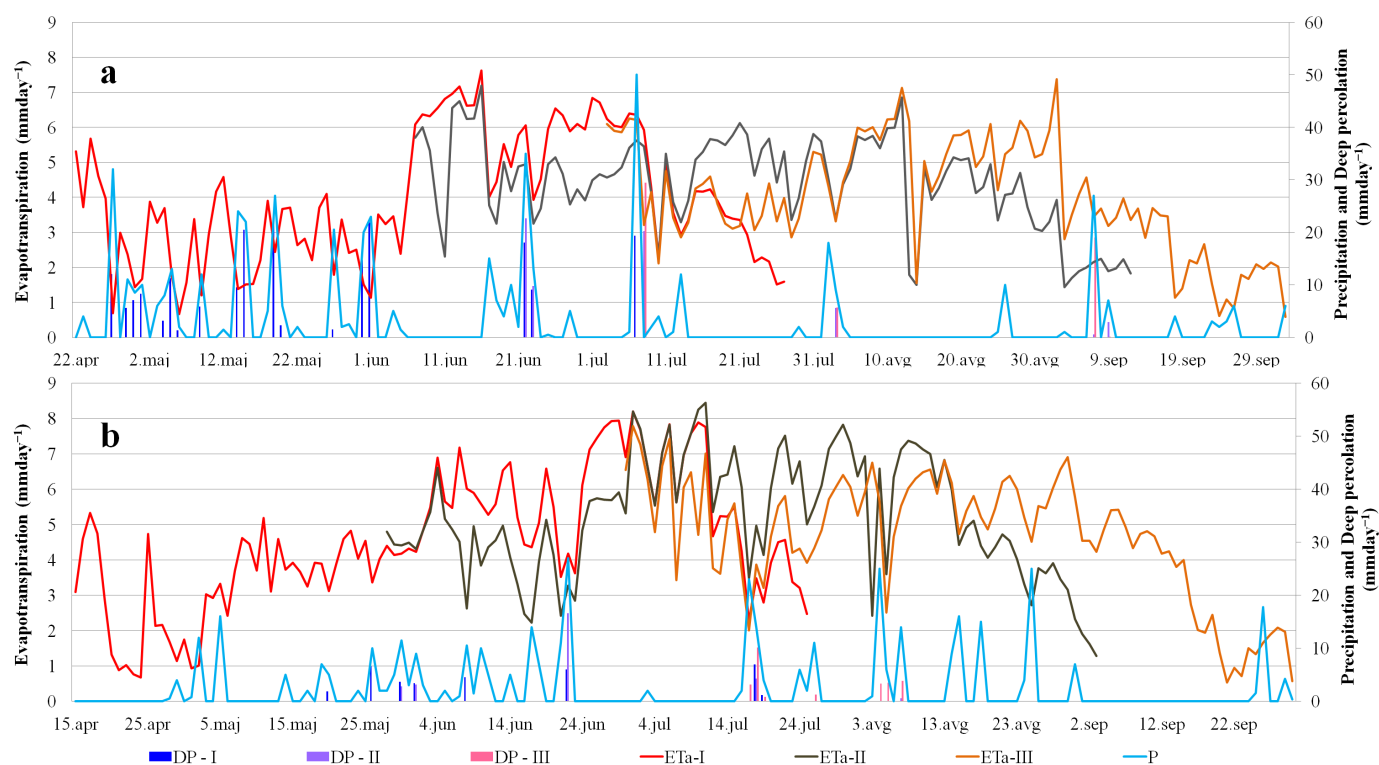


Figure 7. Actual evapotranspiration (ETa), precipitation (P) and deep percolation (DP) among sowing periods of common bean for the 2019 (a) and 2020 (b).

The highest water deficit was observed in the III-F treatment in 2020 (225 mm), and the lowest in sowing period I in 2019, when there was an excess of water due to intense and frequent rainfall, thus no irrigation was applied. On average, the highest water needs were noted in sowing period III (184 mm), and the lowest irrigation needs were noted in sowing period I, approximately 57 mm.

3.3. Soil Moisture

Figure 8a,b show the soil moisture levels in 2019 and 2020, on the days of UAV deployment. The highest soil moisture during the two-year study period was recorded for treatment F, amounting to 30.75% on average, followed by treatment R, 27.25%, and treatment S, 23.66%_{vol}, indicating that at times treatment S caused the plants to be exposed to a mild water stress. In the case of F and R, water availability was generally good.

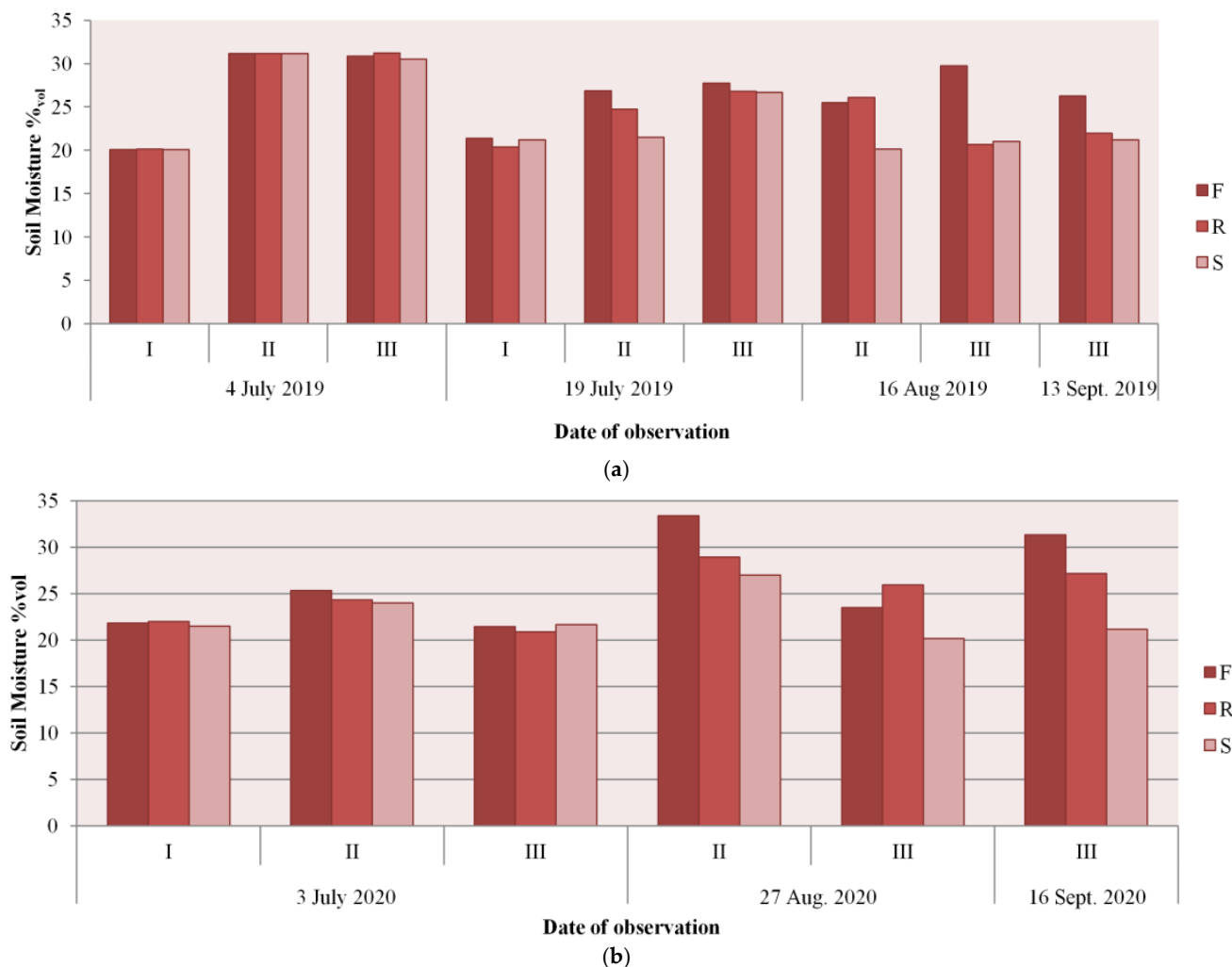


Figure 8. (a) Soil moisture per UAV imagery in 2019. (b) Soil moisture per UAV imagery in 2020 for the F, R and S treatments in three sowing periods (I, II, and III).

3.4. Leaf Area Index (LAI)

Figure 9 shows the leaf area index (LAI) trends by irrigation treatment and sowing period. In 2019, the average maximum values of LAI were uniform, amounting to 3.55 mm^{-2} , 3.57 mm^{-2} , and 3.50 mm^{-2} for treatments F, R, and S, respectively. In the second period, the corresponding values of LAI were 2.8 mm^{-2} , 2.65 mm^{-2} , and 2.41 mm^{-2} and in the third period they were 3.02 , 2.59 , and 2.21 . In the first period of the following year, the average maximum values of LAI were 3.67 mm^{-2} , 3.51 mm^{-2} and 3.21 mm^{-2} for treatments F, R and S, respectively. The corresponding values in the second period were 3.71 mm^{-2} , 3.55 mm^{-2} and 3.11 mm^{-2} , respectively, and in the third period they were 3.98 , 3.95 , and 3.78 , respectively.

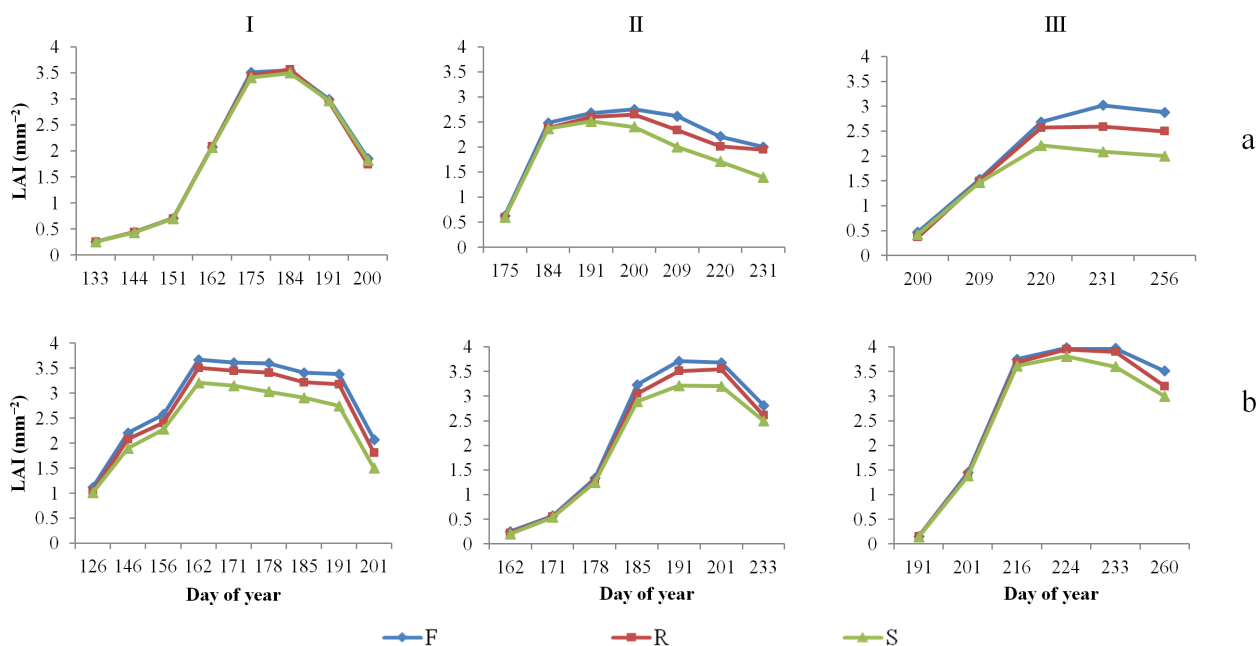


Figure 9. Leaf area index (LAI) by irrigation treatments (F, R and S) and sowing periods (I, II, and III) in 2019 (a) and 2020 (b).

3.5. Vegetation Index Sensitivity to Irrigation Treatment

Table 5 shows Pearson’s coefficients of correlation between the VIs and growth indicators (CC, LAI, soil moisture) of the common bean. NDVI and MCARI11 generally exhibited the best results for all three irrigation treatments. The correlations between NDVI and CC/LAI of the three sowing periods were uniform and varied from 0.94–0.95 to 0.79–0.74, respectively. The correlations between MCARI11 and CC/LAI were also strong, 0.83–0.84 (CC) and 0.71–0.56 (LAI). There was a strong correlation between transpiration and NDVI/MCARI11. The results of the other indices were also satisfactory. For example, the correlation between GNDVI and CC/LAI/T was strong. However, the correlation between soil moisture and the tested parameters was weak negative.

Table 5. Pearson’s coefficients of correlation between average VIs and observed parameters (CC, LAI, soil moisture), and reference and actual evapotranspiration (ET_0 , ET_n).

Irrigation	F				R				S			
	CC	LAI	T	Sm	CC	LAI	T	Sm	CC	LAI	T	Sm
NDVI	0.94 **	0.79 **	0.71 **	−0.29 ns	0.95 **	0.79 **	0.67 **	−0.48 **	0.94 **	0.74 **	0.62 **	−0.61 **
MCARI11	0.83 **	0.71 **	0.78 **	−0.31 *	0.84 **	0.68 **	0.59 **	−0.53 **	0.83 **	0.56 **	0.52 **	−0.60 **
NDRE	0.71 **	0.57 **	0.53 **	−0.34 *	0.71 **	0.53 **	0.44 **	−0.59 **	0.67 **	0.39 **	0.38 **	−0.60 **
GNDVI	0.66 **	0.51 **	0.55 **	−0.34 *	0.66 *	0.49 **	0.45 **	−0.46 **	0.64 **	0.40 **	0.41 **	−0.51 **
OSAVI	0.45 **	0.55 **	0.36 *	−0.42 **	0.41 **	0.47 **	0.37 *	−0.49 **	0.38 *	0.45 **	0.39 **	−0.70 **

Note: *, ** and ns denote $p < 0.05$, $p < 0.001$ and “not significant”, respectively.

3.6. Mapping of Vegetation Indices for Spatial Presentation

NDVI showed the best correlation with CC and LAI of the different sowing periods in all irrigation treatments. As such, it was selected to examine its spatial variation and differences between irrigation treatments and sowing periods in the same periods of 2019 and 2020 (Figure 10). Regarding the treatments, NDVI averages varied from 0.28 to 0.90. These large differences were caused by different sowing periods because the plants were in different phenological stages. The common bean of the first sowing period was in the flowering and pod formation stage, of the second sowing period it was in the intensive growth stage, and of the third sowing period it was in the sprouting stage. The NDVI of the first sowing period in 2019 varied from 0.84 (treatment F) to 0.65 (treatment S), while in

the same period of 2020 it ranged from 0.90 (F) to 0.83 (S). The NDVI of the second sowing period in 2019 varied from 0.54 (F) to 0.42 (S). It was much higher in the same period of 2020, from 0.82 (F) to 0.71 (R). The higher NDVI values in the second period of 2020 were due to more favorable weather conditions and slightly earlier sowing. The treatments for sowing period III, at a given time, were in the sprouting stage, such that their values corresponded to the NDVIs of bare soil [58].

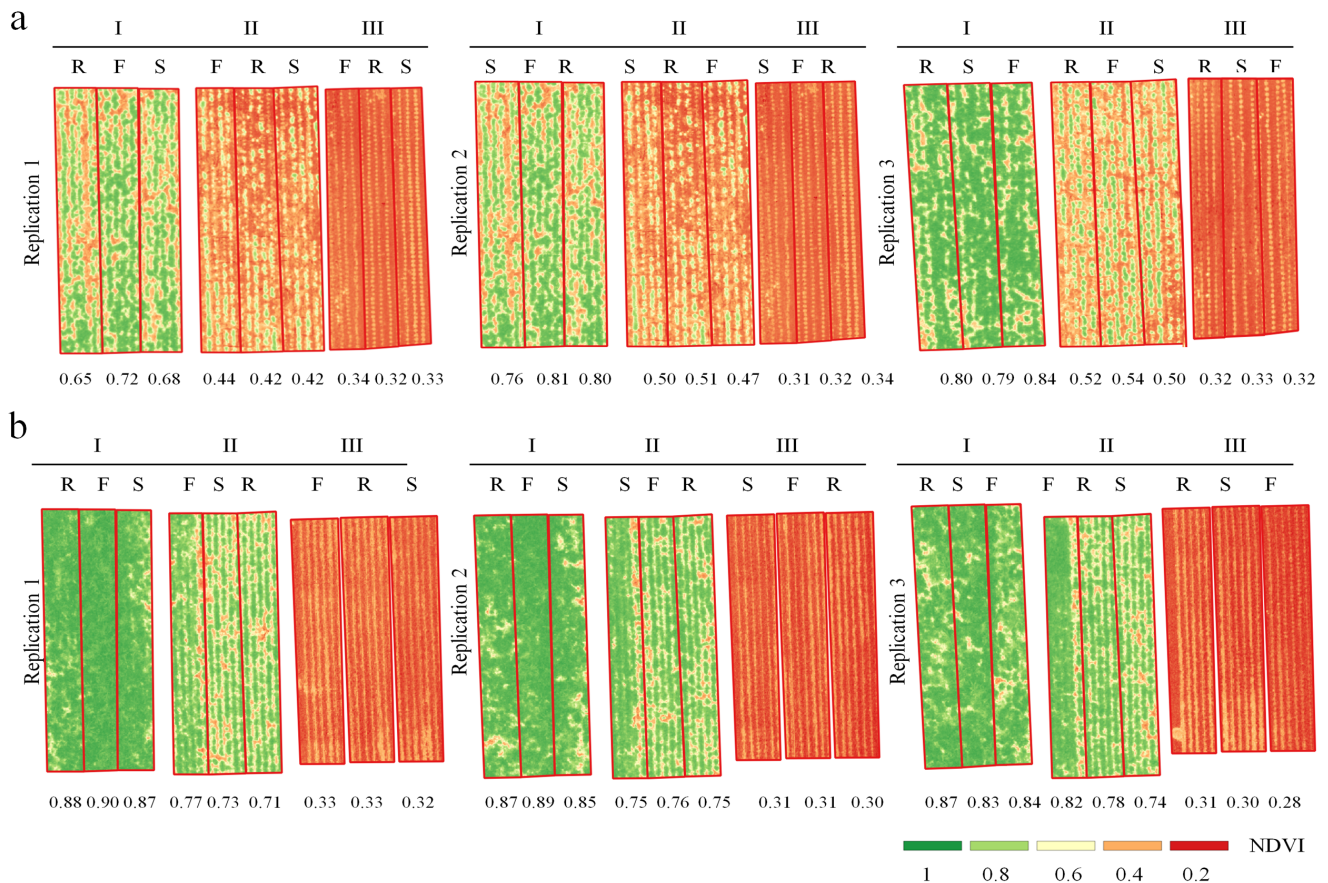


Figure 10. Average NDVI by irrigation treatments (F, R and S) and sowing periods (I, II, and III) on 4 July 2019 (a) and 3 July 2020 (b).

3.7. Response of LAI, CC and VI to Sowing Period and Irrigation Treatment

Table 6 shows the ANOVA test of the studied VIs by treatment and sowing period for 2019 and 2020. In the intensive growth and full development stages, CC, LAI and VI responded differently to the irrigation treatments and sowing periods. In 2019, the LAI of treatment S differed considerably in periods II and III ($p < 0.05$ and $p < 0.01$). Among the VIs, the top performers were NDVI and MCARI11, because they were able to track differences in II-S and III-S ($p < 0.05$). Among the other VIs, GNDVI responded well to III-S ($p < 0.05$) but showed no differences for the other treatments. In 2020, the LAI of treatment S differed considerably in all sowing periods ($p < 0.05$ and $p < 0.01$) while in sowing periods II and III LAI differed among all irrigation treatments. Vegetation indices (VI) could detect water stress in sowing period I, except that there was only one image acquisition, but NDVI, MCARI1 and GNDVI were able to track differences in II-S and III-S ($p < 0.05$).

Table 6. Partial ANOVA table of variables by sowing period and irrigation treatment (2019 and 2020).

Treatment 2019	CC	Yield	LAI	NDVI	MCARI11	GNDVI	OSAVI	NDRE
I-F	ns	ns	ns	ns	ns	ns	ns	ns
I-R	ns	ns	ns	ns	ns	ns	ns	ns
I-S	ns	ns	ns	ns	ns	ns	ns	ns
II-F	ns	ns	ns	ns	ns	ns	ns	ns
II-R	ns	*	*	ns	ns	ns	ns	ns
II-S	*	*	*	*	*	ns	ns	ns
III-F	ns	ns	ns	ns	ns	ns	ns	ns
III-R	ns	ns	ns	ns	ns	ns	ns	ns
III-S	*	*	*	*	*	*	ns	ns
2020								
I-F	ns	ns	ns	ns	ns	ns	ns	ns
I-R	*	ns	ns	ns	ns	ns	ns	ns
I-S	*	**	*	*	*	*	ns	ns
II-F	ns	ns	ns	ns	ns	ns	ns	ns
II-R	ns	**	*	ns	ns	ns	ns	ns
II-S	*	**	*	*	*	*	ns	ns
III-F	ns	ns	ns	ns	ns	ns	ns	ns
III-R	ns	**	*	ns	ns	ns	ns	ns
III-S	*	**	*	*	*	*	ns	ns

Note: *, ** and ns denote $p < 0.05$, $p < 0.001$ and “not significant”, respectively.

NDVI and MCARI11 responded to the differences in LAI in the intensive growth, flowering and reproductive stages, where there was water deficit and temperature stress of the crop (Tmax. 37 °C). By contrast, the response of OSAVI and NDRE to the various irrigation treatments and sowing periods was poor.

3.8. Yield Prediction via Vegetation Indices

Average common bean yields differed significantly by sowing period, from 4.43 tha⁻¹ (IF) to 0.77 tha⁻¹ (IIS). The results indicated that treatments R and S provided the highest water productivity (data non shown), which recommended them as optimal deficit irrigation strategies.

The VIs responded differently to the irrigation treatments and sowing periods (Table 6), and thus affected yield predictions (Table 7). NDVI and MCARI11 could be used for valid predictions based on II-S and III-S data. GNDVI allowed yield prediction only for III-S. Due to the specific features of the year and number of drone sorties (collected VI data), treatments III-R resulted in no stress such that the use of VIs would not have provided valid yield predictions.

Table 7. Mean vegetation indices and yield prediction for common bean under different irrigation treatments and sowing periods.

Treatment	NDVI				MCARI11				GNDVI			
	Mean	SD	Model	r ²	Mean	SD	Model	r ²	Mean	SD	Model	r ²
I-F	0.79	0.07	ns		0.57	0.08			0.92	0.06	ns	
I-R	0.77	0.16	ns		0.54	0.09			0.90	0.05	ns	
I-S	0.67	0.3	ns		0.53	0.01			0.91	0.02	ns	
II-F	0.67	0.09	ns		0.48	0.09			0.81	0.04	ns	
II-R	0.63	0.04	ns		0.45	0.3			0.75	0.03	ns	
II-S	0.56	0.11	y = 794.91x + 3910	0.42	0.39	0.1	y = 379.89x + 3716	0.25	0.67	0.14	ns	
III-F	0.63	0.04	ns		0.55	0.04	ns		0.82	0.04	ns	
III-R	0.61	0.08	ns		0.54	0.08	ns		0.77	0.05	ns	
III-S	0.51	0.10	y = 791.24x + 3655	0.57	0.42	0.01	y = 320.14x + 3501	0.20	0.65	0.12	y = 472.18x + 3543	0.32

The established regression models were validated using 2020 yields. Based on the yield prediction regression models, the performance of NDVI, MCARI11 and GNDVI of treatments II-S and III-S varied (Table 8). The NDVI and MCARI11 of treatment II-S predicted yields better ($r^2 = 0.65$, $y = 4.01 \text{ tha}^{-1}$; $r^2 = 0.70$, $y = 4.28 \text{ tha}^{-1}$) than of the third sowing periods ($r^2 = 0.012$, $y = 3.54 \text{ tha}^{-1}$; $r^2 = 0.020$, $y = 3.7 \text{ tha}^{-1}$). The GNDVI of III-S had a somewhat lower value of RMSE compared to NDVI.

Table 8. Yield model performance based on NDVI, MCARI11 and GNDVI by treatment.

Treatment	NDVI			MCARI11			GNDVI		
	Yield ^a	r^2	p	Yield	r^2	P	Yield	r^2	p
I-F	ns	ns	ns	ns	ns	ns	ns	ns	ns
I-R	ns	ns	ns	ns	ns	ns	ns	ns	ns
I-S	ns	ns	ns	ns	ns	ns	ns	ns	ns
II-F	ns	ns	ns	ns	ns	ns	ns	ns	ns
II-R	ns	ns	ns	ns	ns	ns	ns	ns	ns
II-S	4.01	0.65	0.01	4.28	0.70	0.012	ns	ns	ns
III-F	ns	ns	ns	ns	ns	ns	ns	ns	ns
III-R	ns	ns	ns	ns	ns	ns	ns	ns	ns
III-S	3.54	0.012	0.02	3.62	0.020	0.018	3.7	0.14	0.35

^a Yield—in tha^{-1} .

4. Discussion

The irrigation treatments resulted in the highest rates of transpiration due to the larger amount of water readily available to the common bean [55]. The second sowing period recorded the highest averages due to high temperatures during the period of growth. Evaporation was uniform among the irrigation treatments, but the highest rates were achieved for the second sowing period, when the plants were exposed to high temperatures during germination and sprouting. These findings are consistent with the results reported for late sowing of maize by Srivastava et al. [56] and common bean by Lipovac et al. [57].

The ratio between precipitation and actual evapotranspiration clearly shows when the greatest water deficit occurred. In the first sowing period (I) in 2019, there was no water deficit and irrigation was absent. By contrast, deep percolation was up to 147 mm. The lower consumption of water for the evapotranspiration compared to water income from precipitation is attributable saturation (MVK) when the common bean (plant) has minimized transpiration processes. Also, in this period the temperatures were lower, with multi-day cloudy weather and precipitation. In the second year of research, there was less deep percolation due to more evenly distributed precipitation.

As expected, the soil moisture of treatment F was the highest, but in the cases of deficit irrigation (R and S), regardless of sowing period, the common bean was not under major stress for prolonged periods due to favorable rainfall distributions in 2019 and 2020. Vasic et al. [59] studied common bean growing in Serbia and found that when the distribution of rainfall was adequate, this plant could be grown successfully as an aftercrop without irrigation.

The leaf area index (LAI) is an important indicator because it reflects the environment in which the crop grows [60]. In the case of annual plants, if there is no stress, LAI increases through to the reproductive stage and then decreases as leaves gradually wilt at maturity. In the present study, LAI varied significantly (<0.05) among the sowing periods, but also the irrigation treatments (<0.05) of the second and third sowing periods (treatments S and R). No significant differences were noted in the first period. Regarding the LAI trend, late sowing periods (II and III) resulted in the plant reaching maximum growth quicker and shedding fewer leaves. The LAI at maturity (Figure 9) was higher due to larger amounts of rainfall during that period. In 2019 (sowing periods II and III), LAI was somewhat lower due to a mild water deficit but mostly because of high maximum temperatures ($T_{\text{max}} 37 \text{ }^\circ\text{C}$) at the intensive growth and flowering stages, which caused the common bean to

enter the reproductive stage sooner. In 2020, the maximum values of LAI were uniform among the sowing periods and ranged from 3.97 mm^{-2} to 3.21 mm^{-2} . The differences caused by the different irrigation treatments, weather conditions, and sowing periods were reflected in yields, consistent with the common bean LAIs reported by Karimzadeh et al. [55], Heshmat [61], Rai et al. [43] and Boydston et al. [62] who were dealing with different irrigation strategies.

Vegetation indices are commonly used to monitor crop growth and detect drought and abiotic stress. The VI values in the present study exhibited a trend similar to LAI. Namely, they increased as the biomass grew, through to the reproductive stage, followed by ageing and the increased visibility of bare soil, as reported with regard to other crops by Duchemin et al. [63] and Toureiro et al. [64]. The VIs sensitive to LAI were suitable for yield prediction. There were no significant yield, LAI, CC and VI variations in the first sowing period, regardless of irrigation treatment. This was due to the amount and distribution of rainfall in 2019 (Figure 5a), which was such that no irrigation was required for the first sowing period. There have been similar circumstances under other climate conditions and with different crops [65]. The second and third sowing period (2019, 2020) exhibited significant ($p < 0.05$) differences in yield among the irrigation treatments R and S, mirrored by LAI. However, among the VIs, only NDVI, MCARI11 and GNDVI reflected differences among treatments S. These results were due to the fact that in certain observation periods, the plants experienced no water deficit under treatments F and R, due to irrigation scheduling and weather conditions. In 2019, the differences in maximum NDVI during growth were moderate. The lowest mean NDVI was observed in III-S, and the highest in I-F (Table 7). The highest NDVI (0.89) among the treatments was recorded in the flowering and pod filling stages. Similar values were obtained by Nemeskéri et al. [37] on snap bean (NDVI = 0.85) and Rai et al. [43] on common bean (NDVI = 0.84) and Rinaldi [66] on tomato (NDVI = 0.81). In the same period, GNDVI exhibited the highest values and the trends of MCARI11 and GNDVI were similar.

Even though the difference between the irrigation treatments is obvious (Table 1), there were many times where rainfall just before irrigation treatments R and S created favorable conditions for common bean growth and development while saving water, which resulted in high yields in those treatments. The significant differences between the three sowing periods, despite favorable amounts and distributions of rainfall, were likely due to high temperatures during the flowering and reproductive stages of sowing periods II and III, resulting in reduced pollination efficiency and pod abscission. In their study on the effect of high temperatures and drought stress on common bean, Monterroso et al. [67], Konsens [68] and Herrera [69] drew similar conclusions. In the present research, the sowing period had a significant effect (<0.01) on the yield of the common bean, but due to specific weather conditions (good rainfall distribution), there were no significant differences between the yields of treatments IIF and IIR, suggesting that common bean can be grown effectively under mild water stress (Table 6).

A strong correlation was established between NDVI/MCARI11/GNDVI and LAI under the different irrigation treatments, indicating that VIs can be very useful for non-destructive monitoring of crop status and yield prediction. Similar coefficients of correlation between NDVI and LAI ($r = 0.85$) were reported by Hoffman et al. [70], who studied irrigated barley. Strong correlations between NDVI ($r = 0.90$)/GNDVI ($r = 0.96$) and LAI were established by Lelong et al. [71] with wheat and Rai et al. [43] with common bean. Rinaldi et al. [66] also reported a significant correlation between LAI and NDVI in irrigated snap bean in dry years ($r = 0.82$ and $r = 0.95$). In the present study, a higher sensitivity of LAI to yield, compared to the VIs, stems from the fact that LAI was monitored every 7–10 days during growth, which facilitated the tracking of crop development under different treatments. To determine yields more accurately by using UAVs, the objective of future research will be to increase the number of aerial image acquisition sorties during the season, especially in the intensive growth stage and at times when the crop is exposed to drought stress. The VIs were still useful for tracking the status and predicting yields of

the common bean by irrigation treatment and sowing period. Furthermore, a satisfactory correlation was established between the VIs (NDVI and MCARI11) and transpiration of the common bean, suggesting that these indices can be used to assess crop transpiration and evapotranspiration.

The study showed that NDVI, MCARI1 and GNDVI were solid indices for predicting the yields of treatments II-S because they were able to detect the water stress responsible for reduced yields. Somewhat better results were reported by Spitzkó et al. [72] and da Silva et al. [73]. In addition, Ranjan et al. [44] proposed using NDVI and report $r = 0.62$, as well as $r = 0.54$ for GNDVI, with regard to pinto bean yield prediction. Zhou et al. [40] recommend GNDVI to identify and track drought stress, as well as predict pinto bean yields, as they established strong correlations between that index and yield (0.7 for the early stage of growth and 0.87 mid-growth). Increment in number of UVA could potentially lead to better yield prediction of common bean. In the present research, significantly lower correlation coefficients of sowing period III were due to an unexpected decrease in yield caused by an invasion of forest bugs (*Pentatoma rufipes*) in the reproductive stage, which slowed down pod formation and extended the reproductive stage. Given that the insects did not damage the leaves, only the pods, there was no VI response. Even though the results indicated that the spectral reflection of the vegetation cover can be consistent with LAI and CC, the VIs can be highly effective for predicting yields by sowing period and irrigation treatment. However, pests cannot be detected in some cases based on the VIs, so in situ inspection of the crop is indispensable. Hunt et al. [74] studied the damage caused by potato beetles and found that it was difficult to identify an insect attack based on NDVI. They detected damage by object-based image analysis but indicated that reliable results required a lot of effort.

The spatial variation of NDVI by sowing period and irrigation treatment is shown in Figure 10. A color scale describes the crop status in the field. For example, the plants that were not exposed to water stress exhibited a high NDVI and their color is bright green. Mapping the water deficit of irrigated crops, Veysi et al. [75] and Stone et al. [39] concluded that NDVI was a good indicator of spatial differences in water stress during the entire season. The value of this index also depended on the phenological stage, such that the green color that represents biomass and the red color that represents bare soil can provide insight into the correlation with CC and LAI, and potentially be used to monitor phenological stages by sowing period, as reported by [76–78].

A spatial representation of VIs is useful in many ways from a data interpretation perspective. Namely, if a person lacking knowledge about agricultural activities tries to interpret the data, they may arrive at the wrong conclusions. For example, a low NDVI (say 0.3) might be indicative of a severe drought or lack of nitrogen (yellow leaves), but instead it reflects a late sown crop whose LAI and CC are lower. Therefore, it is extremely important to correlate CC/LAI/T/SM with VIs to assess crop status over an extended area.

5. Conclusions

This research showed that the growth and water supply of the common bean, by sowing period and irrigation treatment, can be monitored by multispectral UAV imagery. Strong correlations were established between VIs and LAI, CC and T. The correlation with soil moisture ranged from strong to satisfactory. The results indicate that NDVI, MCARI1 and GNDVI can correlate strongly with ground parameters (LAI, CC, yield, and T). A low-flying UAV proved to be useful for monitoring crop status and predicting yield and water stress by sowing period and irrigation treatment. However, it is still necessary to collect information in the field in order to ensure better data interpretation. With that prerequisite in mind, the rapid acquisition of reliable data by remote sensing can reduce labor requirements and thus cut operating costs. NDVI, MCARI1 and GNDVI appeared to be reliable indices for predicting common bean yields by sowing period and irrigation treatment. However, remote sensing did not reveal a pest invasion, so that adequate yield predictions require observations in the field or object-based image analysis. The VIs from

the UAV could be used for early water stress detection, irrigation scheduling, irrigation uniformity and spatial crop monitoring. More UAV sorties would have provided better insight into the differences in water deficit between the phenological stages of the common bean, and consequently more reliable assessments of all the studied cases. For more accurate monitoring of water stress and better yield prediction, future research should be based on timely and more frequent drone observations. Expanding the research in terms of pairing the application of a multispectral camera together with a thermal camera could improve the detection of water stress and enhance the yield prediction equation of common bean.

Author Contributions: Conceptualization, A.L. and R.S.; methodology, A.L., R.S., M.Ć., A.B. and P.B.; investigation, A.L., M.Ć., A.B. and P.B.; resources, D.M.; data curation, M.Ć., D.M. and N.D.; writing—original draft preparation, A.L.; writing—review and editing, R.S.; visualization, A.L. and M.Ć.; supervision, N.D. and D.M.; All authors have read and agreed to the published version of the manuscript.

Funding: The paper was produced within the scope of the 451-03-68/2022-14/200116 project funded by the Serbian Ministry of Education, Science and Technological Development.

Data Availability Statement: Not applicable.

Acknowledgments: The authors express their gratitude to the company Napredak A.D. from Stara Pazova for making their experimental field available for the present research. The paper was produced within the scope of the 451-03-68/2022-14/200116 project funded by the Serbian Ministry of Education, Science and Technological Development.

Conflicts of Interest: The authors declare that they have no conflicts of interest.

References

- Forzieri, G.; Feyen, L.; Russo, S.; Voutsoukas, M.; Alfieri, L.; Outten, S.; Migliavacca, M.; Bianchi, A.; Rojas, R.; Cid, A. Multi-hazard assessment in Europe under climate change. *Clim. Chang.* **2016**, *137*, 105–119. [[CrossRef](#)]
- Stričević, R.; Srdjević, Z.; Lipovac, A.; Prodanović, S.; Petrović-Obradović, O.; Čosić, M.; Djurović, N. Synergy of experts' and farmers' responses in climate-change adaptation planning in Serbia. *Ecol. Indic.* **2020**, *116*, 106481. [[CrossRef](#)]
- Fereres, E.; Soriano, M.A. Deficit irrigation for reducing agricultural water use. *J. Exp. Bot.* **2007**, *58*, 147–159. [[CrossRef](#)]
- Zhang, H.; Ma, L.; Douglas-Mankin, K.R.; Han, M.; Trout, T.J. Modeling maize production under growth stage-based deficit irrigation management with RZWQM2. *Agric. Water Manag.* **2021**, *248*, 106767. [[CrossRef](#)]
- Eyni-Nargeseh, H.; AghaAlikhani, M.; Shirani Rad, A.H.; Mokhtassi-Bidgoli, A.; Modarres Sanavy, S.A.M. Late season deficit irrigation for water-saving: Selection of rapeseed (*Brassica napus*) genotypes based on quantitative and qualitative features. *Arch. Agron. Soil Sci.* **2019**, *66*, 126–137. [[CrossRef](#)]
- Comas, L.H.; Trout, T.J.; DeJonge, K.C.; Zhang, H.; Gleason, S.M. Water productivity under strategic growth stage-based deficit irrigation in maize. *Agric. Water Manag.* **2019**, *212*, 433–440. [[CrossRef](#)]
- Čosić, M.; Stričević, R.; Djurović, N.; Lipovac, A.; Bogdan, I.; Pavlović, M. Effects of irrigation regime and application of kaolin on canopy temperatures of sweet pepper and tomato. *Sci. Hortic. (Amst.)* **2018**, *238*, 23–31. [[CrossRef](#)]
- Bogale, A.; Nagle, M.; Latif, S.; Aguila, M.; Müller, J. Regulated deficit irrigation and partial root-zone drying irrigation impact bioactive compounds and antioxidant activity in two select tomato cultivars. *Sci. Hortic.* **2016**, *213*, 115–124. [[CrossRef](#)]
- Adu, M.O.; Yawson, D.O.; Armah, F.A.; Asare, P.A.; Frimpong, K.A. Meta-analysis of crop yields of full, deficit, and partial root-zone drying irrigation. *Agric. Water Manag.* **2018**, *197*, 79–90. [[CrossRef](#)]
- Al-Ghobari, H.M.; Dewidar, A.Z. Integrating deficit irrigation into surface and subsurface drip irrigation as a strategy to save water in arid regions. *Agric. Water Manag.* **2018**, *209*, 55–61. [[CrossRef](#)]
- Ayars, J.E.; Fulton, A.; Taylor, B. Subsurface drip irrigation in California—Here to stay? *Agric. Water Manag.* **2015**, *157*, 39–47. [[CrossRef](#)]
- Saleem, H.; Zaidi, S.J. Recent developments in the application of nanomaterials in agroecosystems. *Nanomaterials* **2020**, *10*, 2411. [[CrossRef](#)] [[PubMed](#)]
- Guerrero, A.; De Neve, S.; Mouazen, A.M. Data fusion approach for map-based variable-rate nitrogen fertilization in barley and wheat. *Soil Tillage Res.* **2021**, *205*, 104789. [[CrossRef](#)]
- Wu, D.; Xu, X.; Chen, Y.; Shao, H.; Sokolowski, E.; Mi, G. Effect of different drip fertigation methods on maize yield, nutrient and water productivity in two-soils in Northeast China. *Agric. Water Manag.* **2019**, *213*, 200–211. [[CrossRef](#)]
- Bateman, N.R.; Catchot, A.L.; Gore, J.; Cook, D.R.; Musser, F.R.; Irby, J.T. Effects of planting date for soybean growth, development, and yield in the Southern USA. *Agronomy* **2020**, *10*, 596. [[CrossRef](#)]

16. Mirshekari, M.; Hosseini, N.M.; Amiri, R.; Zandvakili, O.R. Study the Effects of Planting Date and Low Irrigation. *Rom. Agric. Res.* **2012**, *29*, 189–199.
17. Tunc, M.; Bicer, B.T.; Turk, Z. Cultivation Possibilities of Some Common Beans Varieties Under Second Crop Conditions. *Cercet. Agron. Mold.* **2020**, *53*, 144–151. [[CrossRef](#)]
18. Zeleke, K.; Nendel, C. Growth and yield response of faba bean to soil moisture regimes and sowing dates: Field experiment and modelling study. *Agric. Water Manag.* **2019**, *213*, 1063–1077. [[CrossRef](#)]
19. Delalieux, S.; Somers, B.; Hereijgers, S.; Verstraeten, W.W.; Keulemans, W.; Coppin, P. A near-infrared narrow-waveband ratio to determine Leaf Area Index in orchards. *Remote Sens. Environ.* **2008**, *112*, 3762–3772. [[CrossRef](#)]
20. Agam, N.; Cohen, Y.; Berni, J.A.J.; Alchanatis, V.; Kool, D.; Dag, A.; Yermiyahu, U.; Ben-Gal, A. An insight to the performance of crop water stress index for olive trees. *Agric. Water Manag.* **2013**, *118*, 79–86. [[CrossRef](#)]
21. Poirier-Pocovi, M.; Volder, A.; Bailey, B.N. Modeling of reference temperatures for calculating crop water stress indices from infrared thermography. *Agric. Water Manag.* **2020**, *233*, 106070. [[CrossRef](#)]
22. Moriana, A.; Pérez-López, D.; Prieto, M.H.; Ramírez-Santa-Pau, M.; Pérez-Rodríguez, J.M. Midday stem water potential as a useful tool for estimating irrigation requirements in olive trees. *Agric. Water Manag.* **2012**, *112*, 43–54. [[CrossRef](#)]
23. Lipan, L.; Issa-Issa, H.; Moriana, A.; Zurita, N.M.; Galindo, A.; Martín-Palomo, M.J.; Andreu, L.; Carbonell-Barrachina, Á.A.; Hernández, F.; Corell, M. Scheduling regulated deficit irrigation with leaf water potential of cherry tomato in greenhouse and its effect on fruit quality. *Agriculture* **2021**, *11*, 669. [[CrossRef](#)]
24. Kirnak, H.; Irik, H.A.; Unlukara, A. Potential use of crop water stress index (CWSI) in irrigation scheduling of drip-irrigated seed pumpkin plants with different irrigation levels. *Sci. Hortic.* **2019**, *256*, 108608. [[CrossRef](#)]
25. Weiss, M.; Jacob, F.; Duveiller, G. Remote Sensing for Agricultural Applications: A Meta-Review. *Remote Sens. Environ.* **2020**, *236*, 111402. [[CrossRef](#)]
26. Liaghat, S.; Balasundram, S.K. A Review: The Role of Remote Sensing in Precision Agriculture. *Am. J. Agric. Biol. Sci.* **2010**, *5*, 50–55. [[CrossRef](#)]
27. Shanmugapriya, P.; Rathika, S.; Ramesh, T.; Janaki, P. Applications of Remote Sensing in Agriculture—A Review. *Int. J. Curr. Microbiol. Appl. Sci.* **2019**, *8*, 2270–2283. [[CrossRef](#)]
28. Droogers, P.; Immerzeel, W.W.; Lorite, I.J. Estimating Actual Irrigation Application by Remotely Sensed Evapotranspiration Observations. *Agric. Water Manag.* **2010**, *97*, 1351–1359. [[CrossRef](#)]
29. Belmonte, A.C.; Jochum, A.M.; García, A.C.; Rodríguez, A.M.; Fuster, P.L. Irrigation Management from Space: Towards User-Friendly Products. *Irrig. Drain. Syst.* **2005**, *19*, 337–353. [[CrossRef](#)]
30. Gowda, P.H.; Chávez, J.L.; Colaizzi, P.D.; Evett, S.R.; Howell, T.A.; Tolck, J.A. Remote Sensing Based Energy Balance Algorithms for Mapping ET: Current Status and Future Challenges. *Trans. ASABE* **2007**, *50*, 1639–1644.
31. Mwinuka, P.R.; Mbilinyi, B.P.; Mbungu, W.B.; Mourice, S.K.; Mahoo, H.F.; Schmitter, P. The feasibility of hand-held thermal and UAV-based multispectral imaging for canopy water status assessment and yield prediction of irrigated African eggplant (*Solanum aethiopicum* L.). *Agric. Water Manag.* **2021**, *245*, 106584. [[CrossRef](#)]
32. Yu, N.; Li, L.; Schmitz, N.; Tian, L.F.; Greenberg, J.A.; Diers, B.W. Development of methods to improve soybean yield estimation and predict plant maturity with an unmanned aerial vehicle based platform. *Remote Sens. Environ.* **2016**, *187*, 91–101. [[CrossRef](#)]
33. Li, W.; Niu, Z.; Chen, H.; Li, D.; Wu, M.; Zhao, W. Remote estimation of canopy height and aboveground biomass of maize using high-resolution stereo images from a low-cost unmanned aerial vehicle system. *Ecol. Indic.* **2016**, *67*, 637–648. [[CrossRef](#)]
34. Tunca, E.; Köksal, E.S.; Çetin, S.; Ekiz, N.M.; Balde, H. Yield and leaf area index estimations for sunflower plants using unmanned aerial vehicle images. *Environ. Monit. Assess.* **2018**, *190*, 682. [[CrossRef](#)]
35. Gonzalez-Dugo, V.; Zarco-Tejada, P.; Nicolás, E.; Nortes, P.A.; Alarcón, J.J.; Intrigliolo, D.S.; Fereres, E. Using high resolution UAV thermal imagery to assess the variability in the water status of five fruit tree species within a commercial orchard. *Precis. Agric.* **2013**, *14*, 660–678. [[CrossRef](#)]
36. Virnodkar, S.S.; Pachghare, V.K.; Patil, V.C.; Jha, S.K. *Remote Sensing and Machine Learning for Crop Water Stress Determination in Various Crops: A Critical Review*; Springer: New York, NY, USA, 2020; Volume 21, ISBN 0123456789.
37. Nemeskéri, E.; Molnár, K.; Helyes, L. Relationships of spectral traits with yield and nutritional quality of snap beans (*Phaseolus vulgaris* L.) in dry seasons. *Arch. Agron. Soil Sci.* **2018**, *64*, 1222–1239. [[CrossRef](#)]
38. Hong, M.; Bremer, D.J.; van der Merwe, D. Using Small Unmanned Aircraft Systems for Early Detection of Drought Stress in Turfgrass. *Crop Sci.* **2019**, *59*, 2829–2844. [[CrossRef](#)]
39. Stone, K.C.; Bauer, P.J.; Sigua, G.C. Irrigation management using an expert system, soil water potentials, and vegetative indices for spatial applications. *Trans. ASABE* **2016**, *59*, 941–948. [[CrossRef](#)]
40. Zhou, J.; Khot, L.R.; Boydston, R.A.; Miklas, P.N.; Porter, L. Low altitude remote sensing technologies for crop stress monitoring: A case study on spatial and temporal monitoring of irrigated pinto bean. *Precis. Agric.* **2018**, *19*, 555–569. [[CrossRef](#)]
41. Köksal, E.S.; Erdem, C.; Taşan, M.; Temizel, K.E. Developing New Hyperspectral Vegetation Indexes Sensitive to Yield and Evapotranspiration of Dry Beans. *Turkish J. Agric. For.* **2021**, *45*, 743–749. [[CrossRef](#)]
42. Sankaran, S.; Zhou, J.; Khot, L.R.; Trapp, J.J.; Mndolwa, E.; Miklas, P.N. High-throughput field phenotyping in dry bean using small unmanned aerial vehicle based multispectral imagery. *Comput. Electron. Agric.* **2018**, *151*, 84–92. [[CrossRef](#)]
43. Rai, A.; Sharma, V.; Heitholt, J. Dry bean [*Phaseolus vulgaris* L.] growth and yield response to variable irrigation in the arid to semi-arid climate. *Sustainability* **2020**, *12*, 3851. [[CrossRef](#)]

44. Ranjan, R.; Chandel, A.K.; Khot, L.R.; Bahlol, H.Y.; Zhou, J.; Boydston, R.A.; Miklas, P.N. Irrigated pinto bean crop stress and yield assessment using ground based low altitude remote sensing technology. *Inf. Process. Agric.* **2019**, *6*, 502–514. [[CrossRef](#)]
45. FAOSTAT: FAO Statistical Databases (Food and Agriculture Organization of the United Nations). 2018. Available online: <https://www.fao.org/faostat/en/#home> (accessed on 14 April 2018).
46. Škorić, A.; Filipovski, G.; Čirić, M. Soil Classification of Yugoslavia, Academy of Sciences and Artists of Bosnia and Herzegovina. In *Special Issue, Book LXXVII, Sarajevo*; Academy of Sciences and Arts of Bosnia and Herzegovina: Sarajevo, Bosnia and Herzegovina, 1985. (In Serbian)
47. USDA. *Kellogg Soil Survey Laboratory Methods Manual*; Soil Survey Investigations Report No. 42, Version 5.0; Burt, R., Staff, S.S., Eds.; U.S. Department of Agriculture, Natural Resources Conservation Service: Washington, DC, USA, 2014.
48. Allen, R.G.; Pereira, L.S.; Raes, D.; Smith, M. Crop evapotranspiration: Guidelines for computing crop water requirements. In *FAO Irrigation and Drainage Paper 56*; UN-FAO: Rome, Italy, 1998.
49. Ustuner, M.; Sanli, F.B.; Abdikan, S.; Esetlili, M.T.; Kurucu, Y. Crop type classification using vegetation indices of rapideye imagery. *Int. Arch. Photogramm. Remote Sens. Spatial Inf. Sci.* **2014**, *40*, 195. [[CrossRef](#)]
50. Haboudane, D.; Miller, J.R.; Pattey, E.; Zarco-Tejada, P.J.; Strachan, I.B. Hyperspectral vegetation indices and novel algorithms for predicting green LAI of crop canopies: Modeling and validation in the context of precision agriculture. *Remote Sens. Environ.* **2004**, *90*, 337–352. [[CrossRef](#)]
51. Gitelson, A.; Merzlyak, M.N. Quantitative estimation of chlorophyll-a using reflectance spectra: Experiments with autumn chestnut and maple leaves. *J. Photochem. Photobiol. B Biol.* **1994**, *22*, 247–252. [[CrossRef](#)]
52. Omer, G.; Mutanga, O.; Abdel-Rahman, E.M.; Peerbhay, K.; Adam, E. Mapping leaf nitrogen and carbon concentrations of intact and fragmented indigenous forest ecosystems using empirical modeling techniques and WorldView-2 data. *ISPRS J. Photogramm. Remote Sens.* **2017**, *131*, 26–39. [[CrossRef](#)]
53. Zou, X.; Mottus, M. Sensitivity of common vegetation indices to the canopy structure of field crops. *Remote Sens.* **2017**, *9*, 994. [[CrossRef](#)]
54. SAS *Statistical Package*; SAS Version 9.1.3; SAS Institute Inc.: Cary, NC, USA, 2007.
55. Karimzadeh, H.; Nezami, A.; Kafi, M. Responses of two common bean (*Phaseolus vulgaris* L.) genotypes to deficit irrigation. *Agric. Water Manag.* **2019**, *213*, 270–279. [[CrossRef](#)]
56. Srivastava, R.K.; Panda, R.K.; Chakraborty, A.; Halder, D. Quantitative estimation of water use efficiency and evapotranspiration under varying nitrogen levels and sowing dates for rainfed and irrigated maize. *Theor. Appl. Climatol.* **2020**, *139*, 1385–1400. [[CrossRef](#)]
57. Lipovac, A.; Stričević, R.; Ćosić, M.; Djurović, N. Productive and non-productive use of water of common bean under full and deficit irrigation. *Acta Hortic.* **2022**, *1335*, 635–641. [[CrossRef](#)]
58. Lillesand, T.M.; Kiefer, R.W.; Chipman, J.W. *Remote Sensing and Image Interpretation*; John Wiley & Sons: Hoboken, NJ, USA, 2008.
59. Vasić, M.; Milić, S.; Pejić, B.; Gvozdanović-Varga, J.; Maksimović, L.; Bošnjak, D. The possibility of after production of beans (*Phaseolus vulgaris* L) in the agro-ecological conditions of Vojvodina. *J. Inst. Field Veg. Crops* **2007**, *43*, 283–291.
60. Bréda, N.J.J. Ground-based measurements of leaf area index: A review of methods, instruments and current controversies. *J. Exp. Bot.* **2003**, *54*, 2403–2417. [[CrossRef](#)]
61. Heshmat, K.; Asgari Lajayer, B.; Shakiba, M.R.; Astatkie, T. Assessment of physiological traits of common bean cultivars in response to water stress and molybdenum levels. *J. Plant Nutr.* **2021**, *44*, 366–372. [[CrossRef](#)]
62. Boydston, R.A.; Porter, L.D.; Chaves-Cordoba, B.; Khot, L.R.; Miklas, P.N. The impact of tillage on pinto bean cultivar response to drought induced by deficit irrigation. *Soil Tillage Res.* **2018**, *180*, 63–72. [[CrossRef](#)]
63. Duchemin, B.; Hadria, R.; Erraki, S.; Boulet, G.; Maisongrande, P.; Chehbouni, A.; Escadafal, R.; Ezzahar, J.; Hoedjes, J.C.B.; Kharrou, M.H.; et al. Monitoring wheat phenology and irrigation in Central Morocco: On the use of relationships between evapotranspiration, crops coefficients, leaf area index and remotely-sensed vegetation indices. *Agric. Water Manag.* **2006**, *79*, 1–27. [[CrossRef](#)]
64. Toureiro, C.; Serralheiro, R.; Shahidian, S.; Sousa, A. Irrigation management with remote sensing: Evaluating irrigation requirement for maize under Mediterranean climate condition. *Agric. Water Manag.* **2017**, *184*, 211–220. [[CrossRef](#)]
65. Zhang, H.; Oweis, T. Water-yield relations and optimal irrigation scheduling of wheat in the Mediterranean region. *Agric. Water Manag.* **1999**, *38*, 195–211. [[CrossRef](#)]
66. Rinaldi, M.; Castrignanò, A.; De Benedetto, D.; Sollitto, D.; Ruggieri, S.; Garofalo, P.; Santoro, F.; Figorito, B.; Gualano, S.; Tamborrino, R. Discrimination of tomato plants under different irrigation regimes: Analysis of hyperspectral sensor data. *Environmetrics* **2014**, *26*, 77–88. [[CrossRef](#)]
67. Monterroso, V.A.; Wien, H.C. Flower and Pod Abscission Due to Heat Stress in Beans. *J. Am. Soc. Hortic. Sci.* **2019**, *115*, 631–634. [[CrossRef](#)]
68. Konsens, I.; Ofir, M.; Kigel, J. The Effect of Temperature on the Production and Abscission of Flowers and Pods in Snap Bean (*Phaseolus vulgaris* L.). *Ann. Bot.* **1991**, *67*, 391–399. [[CrossRef](#)]
69. Herrera, M.D.; Reynoso-Camacho, R.; Melero-Meraz, V.; Guzmán-Maldonado, S.H.; Acosta-Gallegos, J.A. Impact of soil moisture on common bean (*Phaseolus vulgaris* L.) phytochemicals. *J. Food Compos. Anal.* **2021**, *99*, 103883. [[CrossRef](#)]
70. Hoffmann, H.; Jensen, R.; Thomsen, A.; Nieto, H.; Rasmussen, J.; Friborg, T. Crop water stress maps for an entire growing season from visible and thermal UAV imagery. *Biogeosciences* **2016**, *13*, 6545–6563. [[CrossRef](#)]

71. Lelong, C.C.D.; Burger, P.; Jubelin, G.; Roux, B.; Labbé, S.; Baret, F. Assessment of unmanned aerial vehicles imagery for quantitative monitoring of wheat crop in small plots. *Sensors* **2008**, *8*, 3557–3585. [[CrossRef](#)]
72. Spitkó, T.; Nagy, Z.; Zsubori, Z.T.; Szőke, C.; Berzy, T.; Pintér, J.; Marton, C.L. Connection between normalized difference vegetation index and yield in maize. *Plant Soil Environ.* **2016**, *62*, 293–298. [[CrossRef](#)]
73. Da Silva, E.E.; Rojo Baio, F.H.; Ribeiro Teodoro, L.P.; da Silva Junior, C.A.; Borges, R.S.; Teodoro, P.E. UAV-multispectral and vegetation indices in soybean grain yield prediction based on in situ observation. *Remote Sens. Appl. Soc. Environ.* **2020**, *18*, 100318. [[CrossRef](#)]
74. Hunt, E.R.; Rondon, S.I. Detection of potato beetle damage using remote sensing from small unmanned aircraft systems. *J. Appl. Remote Sens.* **2017**, *11*, 026013. [[CrossRef](#)]
75. Veysi, S.; Naseri, A.A.; Hamzeh, S.; Bartholomeus, H. A satellite based crop water stress index for irrigation scheduling in sugarcane fields. *Agric. Water Manag.* **2017**, *189*, 70–86. [[CrossRef](#)]
76. Tenreiro, T.R.; García-Vila, M.; Gómez, J.A.; Jiménez-Berni, J.A.; Fereres, E. Using NDVI for the assessment of canopy cover in agricultural crops within modelling research. *Comput. Electron. Agric.* **2021**, *182*, 106038. [[CrossRef](#)]
77. Trout, T.J.; Johnson, L.F.; Gartung, J. Remote sensing of canopy cover in horticultural crops. *HortScience* **2008**, *43*, 333–337. [[CrossRef](#)]
78. Gitelson, A.A. Remote estimation of crop fractional vegetation cover: The use of noise equivalent as an indicator of performance of vegetation indices. *Int. J. Remote Sens.* **2013**, *34*, 6054–6066. [[CrossRef](#)]